Effectiveness Heat Transfer of Combined Convection Flow Ag-TiO_2-GO Water Casson Ternary Hybrid Nanofluids in Magneto-Hydrodynamic Medium

Munirah Alotaibi[1], Mohammed Shqair[2,*], Mohammed Z. Swalmeh[3] and Ahmed Hagag[4]

[1] Department of Mathematical Sciences, College of Science, Princess Nourah bint Abdulrahman University, Riyadh, 11671, Saudi Arabia

[2] Department of Physics, College of Science, Zarqa University, Zarqa, 13110, Jordan

[3] Faculty of Arts and Sciences, Aqaba University of Technology, Aqaba, 77110, Jordan

[4] Department of Basic Science, Faculty of Engineering, Sinai University-Kantara Branch, Ismailia, 41636, Egypt

INFORMATION

Keywords:
Casson fluid (CF)
hybrid nanofluid
viscous dissipation
magneto-hydrodynamic medium
keller box method

DOI: 10.23967/j.rimni.2025.10.59527

SCIPEDIA Revista Internacional de Métodos Numéricos para Cálculo y Diseño en Ingeniería

Revista Internacional Métodos numéricos para cálculo y diseño en ingeniería RIMNI CIMNE

Effectiveness Heat Transfer of Combined Convection Flow Ag-TiO_2-GO Water Casson Ternary Hybrid Nanofluids in Magneto-Hydrodynamic Medium

Munirah Alotaibi[1], **Mohammed Shqair**[2,*], **Mohammed Z. Swalmeh**[3] **and Ahmed Hagag**[4]

[1]Department of Mathematical Sciences, College of Science, Princess Nourah bint Abdulrahman University, Riyadh, 11671, Saudi Arabia

[2]Department of Physics, College of Science, Zarqa University, Zarqa, 13110, Jordan

[3]Faculty of Arts and Sciences, Aqaba University of Technology, Aqaba, 77110, Jordan

[4]Department of Basic Science, Faculty of Engineering, Sinai University-Kantara Branch, Ismailia, 41636, Egypt

ABSTRACT

The chief target of this existing study is to demonstrate and discuss the problem behaviors of ternary hybrid nanofluid (HNF) flow across a vertical sheet. The boundary layer through a Casson medium and magneto-hydrodynamics effects were considered. Besides that, the constant wall temperature boundary conditions were also subjected to the present problem. The non-dimensional dominant equations for the considered problem are studied numerically, and the Keller box method (KBM) is meticulously chosen because of its suitability and accuracy. The outcome linear system of equations was programmed via MATLAB command software. The impact of magnetic, Casson ternary (HNFs), and mixed convection coefficients on the interested physical quantities in this study were obtained as results on the type figures and tables. These work outcomes agree with earlier work outcomes. The outcome linear system of equations was programmed via MATLAB command software. The effects of magnetic, Casson, nanoparticle (NPs) volume fraction, and mixed convection parameters on Nusselt number (Nu), local skin friction, temperature profiles, and velocity profiles were obtained as results from the type figures and tables. As an important result, the parameters enhanced the heat transfer, velocity, and friction when adding (NPs), so the ternary (HNFs) studied in the present study became an efficient fluid. These current work outcomes are in excellent agreement with earlier work outcomes.

OPEN ACCESS

Received: 10/10/2024

Accepted: 07/01/2025

Published: 07/04/2025

DOI
10.23967/j.rimni.2025.10.59527

Keywords:
Casson fluid (CF)
hybrid nanofluid
viscous dissipation
magneto-hydrodynamic medium
keller box method

Abbreviations

Numerical solutions obtained by TAM of fractional order with different values of α, β and μ.

Symbol	Description	Units
U,V	Velocity components along the x- and y-axes	m/s
T	Temperature	K

*Correspondence: Mohammed Shqair (mshqair@zu.edu.jo).

T_w	Wall temperature	K
T_∞	Ambient temperature	K
B_0	Magnetic field strength	T (Tesla)
β	(CF) parameter	–
χ_{Ag}, χ_{TiO_2}, χ_{GO}	Volume fraction of (NPs) (Ag, TiO_2, GO)	–
ρ_{THNF}	Density of ternary (HNF)	kg/m^3
μ_{THNF}	Dynamic viscosity of ternary (HNF)	Pa·s
k_{THNF}	Thermal conductivity of ternary (HNF)	W/m·K
C_f	Skin friction coefficient	–
Nu	Nusselt number	–
σ_{THNF}	Electrical conductivity of ternary (HNFs)	S/m
Pr	Prandtl number	–
Re	Reynolds number	–
M	Magnetic parameter	–
a/c	Stretching sheet parameter	–
λ	Mixed convection parameter	–
η	Similarity variable	–
$f(\eta)$	Dimensionless stream function	–
$\theta(\eta)$	Dimensionless temperature profile	–

1 Introduction

A hybrid nanofluid (HNF) improves thermal properties where different kinds of (NPs) are dispersed inside a base fluid, usually a liquid like water, oil, or ethylene glycol. This amalgamation can enhance thermal conductivity, heat transfer rates, and overall fluid efficiency compared to conventional nanofluids that utilize a singular (NP) type. Incorporating several (NPs) can provide synergistic effects that enhance heat conductivity. Hybrid nanofluids (HNFs) provide enhanced heat transfer properties, rendering them appropriate for cooling systems and renewable energy technologies. The amalgamation of many (NP) kinds can improve suspension stability, mitigating sedimentation and agglomeration challenges. They possess potential uses across multiple domains, including automotive, aerospace, electronics cooling, and others. Yaw et al. [1] described a (HNF) primarily consisting of nanoplatelets of graphene and nanocrystals of cellulose (NPs) floating in distilled water to ethylene glycol. A reverse flow cooler was utilized in assessing the (HNF) thermal performance. Poloju et al. [2] conducted a study on the effects of (HNFs) on the flow efficiency and heat transfer of a thermal exchanger experimentally. The heat transfer efficiency improved to 94% with the utilization of (HNFs). The used (NPs) have superior heat transmission capability relative to the other HNFs. Alwawi et al. [3] tested energy transportation in nanofluids, focusing on the mixed convection flow of a Williamson (HNF).

Almse'adeen et al. [4] studied the properties of mass and heat transmission in Casson Ternary (HNFs), subjected to a magnetic field, at a stable temperature at the wall boundaries. Madiwal et al. [5] examined the capabilities of a Casson (HNF), where ZnO and MoS_2 (NPs) are suspended in the oil of the engine, to improve the chemical properties of a lubricant influence. Akbar et al. [6] examined the physical simulation of Casson (HNF) flow characterized by magnetization and heat radiation, within a laminar, incompressible channel. The (CF) type was named after Casson when he proposed it for the first time [7] in 1959 during an investigation into the rheological properties of pigmented ink. The chemical reaction effect on heat and mass transfer by mixed convection flow of (CF) was considered by El-Kabeir et al. [8] in their study of mixed convective flow. Khan et al. [9] investigated the classical

Graetz problem theoretically using the (CF) model. Solving the flow problem is performed using the bvp4c methodology. Hamarsheh et al. [10] introduced a simulation study of the natural convective flow of a Casson nanofluid along a horizontal cylinder using a methanol-based fluid. The study performed by Yusof et al. [11] focused on investigating the impact of radiation on (CF) flowing through a rapidly accelerated plate, taking into consideration the effects of permeability and slip.

The magnetic field can be utilized to regulate or enhance flow, either diminishing turbulence or augmenting laminar heat transfer. Al-Hanaya et al. [12] examined the conduct of time-dependent (CF), considering magnetohydrodynamics influence and Darcian flow. The impact of viscous dissipation on the pace at which energy is dissipated is a key focus within the Casson model. The interaction between the Casson model and viscous dissipation can result in complex fluid behaviour, causing non-linear temperature gradients and modified flow dynamics. Comprehending this interaction is crucial for effectively forecasting and comprehending the actions of nanofluids in real-world scenarios. Pop et al. [13] study the behavior of a (CF) subjected to dissipation effects and thermal radiation to find the free convection in a square cavity. Khan et al. [14] have examined the behaviour of (CF) in Blasius and Sakiadis flows, taking into account the effects of viscous dissipation. Hayat et al. [15] have provided a detailed analysis of a magneto-hydrodynamic (CF) with changing characteristics including viscous dissipation. Barik et al. [16] investigated the thermal radiation effect on a turbulent magnetohydrodynamic (MHD) flow around an inclined porous heated plate, considering viscous dissipation. Qasim et al. [17] have elucidated the phenomenon of viscous dissipation in the boundary layer flow of (CF), specifically concerning heat transfer over a shrinking permeable strip. Medikare et al. [18] considered the flow of (MHD) (CF) across a non-linear stretching surface with viscous dissipation, specifically focusing on the stagnation point. Moreover, viscous dissipation effect on the overall dynamics of the nanofluid is significant and should not be disregarded [19]. The delicate equilibrium between viscous dissipation and other influential elements, such as thermal conduction and convection, can greatly impact the thermal efficiency of the nanofluid. The complex interaction emphasizes the need of take into account viscous dissipation in the modeling and analysis of nanofluid systems.

The (KBM) is a numerical methodology employed to solve partial differential equations that characterize fluid flow, especially regarding boundary layer issues. This technique is frequently utilized in the Navier-Stokes equations or other associated models in fluid dynamics. It is especially convenient for examining flows with intricate geometries or boundary conditions. Jamshed et al. [20] examined the Casson nanofluid flow under inclined magnetohydrodynamics, Joule heating, incorporating viscous dissipation, thermal radiation, and particle structure factor impacts on a moving smooth horizontal surface, alongside an entropy analysis. Numerically solved these problems via the conventional (KBM). Alwawi et al. [21] examined the intrinsic energy transfer dynamics of a trihybrid Jeffrey nanofluid as it traverses a radiating, magnetized cylinder. The Keller-box method is utilized to estimate the mathematical solution governing the problem. For (HNF) flow over a starching sheet with thermal radiation, Farooq et al. [22] investigated the features of the entropy profiles, thermal fields, and velocities. The carbon nanotubes, specifically single- and multi-walled carbon nanotubes, are employed as (NPs) that exhibit a Cattaneo-Christov heat flux. In this scenario, ethylene glycol is employed as the basis fluid. MATLAB's famous and extremely efficient Keller-box technique was used. Alzu'bi et al. [23] conducted a computational analysis of energy transmission and heat transfer in Casson ternary (HNFs), that incorporate mixed convection flow over a downward stretched sheet. The research investigates Newtonian thermal boundary conditions and the impact of magnetohydrodynamics (MHD). The Keller box numerical approach is employed to provide results with precision and efficiency.

Recently, convection boundary layer flow problems have been widely cared for in fluid dynamics fields applied in industry and engineering. So, heat transfer has been widely used in solar heaters and engine cooling. Moreover, the treatment and improvement of fluids by adding (NPs) were utilized to raise efficiency and gain advantages in industrial and applied fields. Depending on the above literature, this numerical examination exhibits mixed convection in (CTHN) heat transfer characteristics over a magnetic medium vertical stretching sheet. All mathematical transformations for the studied model that govern the stated problem, were presented and solved. Consequentially, the numerical outcomes were discussed, analyzed, and displayed as figures and tables.

The novelty of this study appears in studying the effects of Casson ternary (HNFs) in magneto-hydrodynamic fields, motivated by the previously published works investigated. This work primarily focuses on combined convection flow over a vertical stretched sheet in ternary (HNFs) subjected to a magnetic field. Furthermore, ternary hybrid (NPs), including Silver, Titanium dioxide, and Graphene oxide, are integrated, with water serving as the base fluid. The formulated governing equations for the analyzed problem are transformed into a system of partial differential equations (PDEs) through the application of appropriate similarity transformations. Thus, these PDEs can be solved numerically using the Keller box approach. Various ways exist to obtain numerical and graphical outcomes of the current research; nevertheless, the Keller box strategy is more straightforward for simulation and for developing MATLAB software. This strategy yields more precise findings.

This work arrangement is presented as: problem formulation is considered in Section 2. The numerical method and accuracy are presented in Section 3. Results and discussion are considered in Section 4 where the conclusion of this study is presented in Section 5.

2 Problem Construction

Heat transfer of (CTHN) was studied considering magnetohydrodynamic effects on the vertical stretching sheet. Constant wall temperature boundary conditions were also considered. The (NPs), Ag, TiO_2, GO, suspended in based fluid, Water, were utilized in this investigation. The impacts of the magnetohydrodynamic MHD, Casson, and (NPs) volume fraction were included. As illustrated in Fig. 1, the coordinate geometry is defined in which the ternary (HNF) flows in the form of the x-coordinate and is estimated horizontally over the vertical stretching sheet. Correspondingly, the y-coordinate is gauged by the height orthogonal to the assumed vertical stretching sheet.

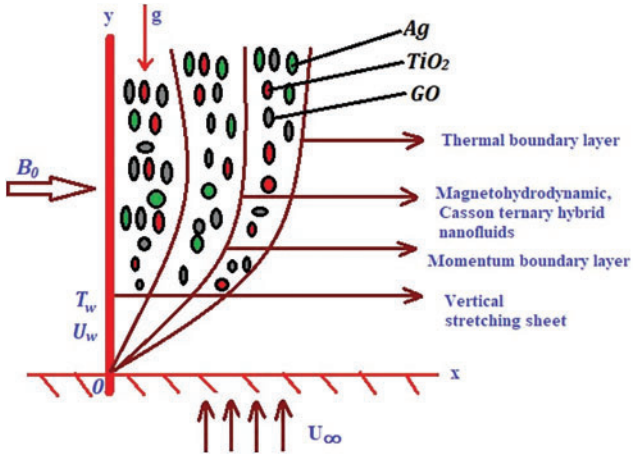

Figure 1: The physical model

By looking at these hypotheses depending on Casson and magnetohydrodynamics influences, besides the tri (HNFs) model, the two-dimensional dominant equations, is [24,25]:

$$\frac{\partial U}{\partial X}+\frac{\partial V}{\partial Y}=0. \tag{1}$$

$$U\frac{\partial U}{\partial X}+V\frac{\partial V}{\partial X}=U_e\frac{\partial U_e}{dX}+\frac{\mu_{THNF}}{\rho_{THNF}}\left(1+\frac{1}{\beta}\right)\frac{\partial^2 U}{\partial Y^2}+(\rho\beta)_{THNF}g\left(T-T_\infty\right)-\frac{\sigma_{THNF}}{\rho_{THNF}}B_0^2\left(U-U_e\right). \tag{2}$$

$$U\frac{\partial T}{\partial X}+V\frac{\partial T}{\partial Y}=\frac{k_{THNF}}{(\rho C_P)_{THNF}}\frac{\partial^2 T}{\partial y^2}. \tag{3}$$

(U,V), T, β, B_0^2, are pointed to velocity components that depend on the directions of X and Y, temperature, Casson parameter, and magnetohydrodynamics field strength, respectively [26,27].

The physical quantities k_{THNF}, μ_{THNF} are defined kinematic and dynamic viscosity, β_{THNF} is the thermal expansion coefficient. $\left(\rho c_p\right)_{THNF}$, σ_{THNF} are called heat capacity and electrical conductivity [28,29]. The subscripts THNF and F are devoted to the ternary (HNF) and based fluid. Two important simulation models such as the Tiwari and Das model [30] and the Buongiorno model [31], respectively, are perpetually used to examine the conduct of nanofluids. In this consideration, Tiwari and Das's model for a nanofluid model with realistic practical liaisons is supposed to analyze the nanofluids' influences on convection flow. This model provides a direct description of nanosubstances' behaviors and characteristics in the same equations, which are distinct from other models, as below [32]:

$$\begin{aligned}
(\mu)_{HTNF} &= \left(1-\chi_{Ag}\right)^{-2.5}\left(1-\chi_{TiO_2}\right)^{-2.5}\left(1-\chi_{GO}\right)^{-2.5}\mu_F,\\
(\rho)_{HTNF} &= \left(1-\chi_{Ag}\right)\left[\left(1-\chi_{TiO_2}\right)\left[\left(1-\chi_{GO}\right)\rho_{\text{water}}+\chi_{Ag}\rho_{Ag}\right]+\chi_{TiO_2}\rho_{TiO_2}\right]+\chi_{GO}\rho_{GO},\\
\left(\rho c_p\right)_{HTNF} &= \left(1-\chi_{Ag}\right)\left[\left(1-\chi_{TiO_2}\right)\left[\left(1-\chi_{GO}\right)\left(\rho c_p\right)_{\text{water}}+\chi_{Ag}\left(\rho c_p\right)_{Ag}\right]+\right.\\
&\quad \left.\chi_{TiO_2}\left(\rho c_p\right)_{TiO_2}\right]+\chi_{GO}\left(\rho c_p\right)_{GO},\\
\frac{k_{THNF}}{k_{HNF}} &= \frac{\left(k_{Ag}+2k_{HNF}\right)-2\chi_{TiO_2}\left(k_{HNF}-k_{TiO_2}\right)}{\left(k_{Ag}+2k_{HNF}\right)+\chi_{Ag}\left(k_{HNF}-k_{Ag}\right)},\\
\frac{k_{HNF}}{k_{NF}} &= \frac{\left(k_{TiO_2}+2k_{NF}\right)-2\chi_{TiO_2}\left(k_{nf}-k_{TiO_2}\right)}{\left(k_{TiO_2}+2k_{NF}\right)+\chi_{TiO_2}\left(k_{NF}-k_{TiO_2}\right)},\\
\frac{k_{NF}}{k_{\text{water}}} &= \frac{\left(k_{GO}+2k_{\text{water}}\right)-2\chi_{GO}\left(k_{\text{Water}}-k_{GO}\right)}{\left(k_{GO}+2k_{\text{water}}\right)+\chi_{GO}\left(k_{\text{Water}}-k_{GO}\right)}\\
\sigma_{HTNF} &= \left[1+\frac{3\left(\left(\sigma_{Ag}/\sigma_{HNF}\right)-1\right)\chi_{Ag}}{\left(\left(\sigma_{Ag}/\sigma_{HNF}\right)+2\right)-\chi_{Ag}\left(\left(\sigma_{Ag}/\sigma_{Hnf}\right)-1\right)}\right]\sigma_{HNF},\\
\sigma_{HNF} &= \left[1+\frac{3\left(\left(\sigma_{TiO_2}/\sigma_{NF}\right)-1\right)\chi_{TiO_2}}{\left(\left(\sigma_{TiO_2}/\sigma_{NF}\right)+2\right)-\chi_{TiO_2}\left(\left(\sigma_{TiO_2}/\sigma_{NF}\right)-1\right)}\right]\sigma_{NF},\\
\sigma_{NF} &= \left[1+\frac{3\left(\left(\sigma_{GO}/\sigma_{\text{water}}\right)-1\right)\chi_{GO}}{\left(\left(\sigma_{GO}/\sigma_{\text{water}}\right)+2\right)-\chi_{GO}\left(\left(\sigma_{GO}/\sigma_{\text{water}}\right)-1\right)}\right]\sigma_{\text{water}}.
\end{aligned} \tag{4}$$

Utilizing the Eq. (4) into Eqs. (1)–(3), then we acquire:

$$\frac{\partial U}{\partial X}+\frac{\partial V}{\partial Y}=0, \tag{5}$$

$$U\frac{\partial U}{\partial X}+V\frac{\partial V}{\partial X}=U_e\frac{\partial U_e}{dX}+\frac{\rho_{\text{Water;}}}{\rho_{\text{THNF}}}\left[\left(1-\chi_{Ag}\right)^{-2.5}\left(1-\chi_{TiO_2}\right)^{-2.5}\left(1-\chi_{GO}\right)^{-2.5}\right]\left(1+\frac{1}{\beta}\right)\frac{\partial^2 U}{\partial Y^2}+$$
$$\left(\frac{1}{\rho_{THNF}}\left(1-\chi_{Ag}\right)\left[\left(1-\chi_{TiO_2}\right)\left[\left(1-\chi_{GO}\right)+\chi_{Ag}\frac{\beta_{Ag}}{\beta_{\text{Water;}}}\right]+\chi_{TiO_2}\frac{\beta_{TiO_2}}{\beta_{\text{water;}}}\right]+\right. \tag{6}$$
$$\left.\chi_{GO}\frac{\beta_{GO}}{\beta_{\text{water;}}}\right)\text{g}\left(T-T_\infty\right)-\frac{\sigma_{THNF}}{\rho_{THNF}}B_0^2\left(U_e-U\right),$$

$$U\frac{\partial T}{\partial X}+V\frac{\partial T}{\partial Y}$$
$$=\frac{1}{Pr}\left(\frac{\frac{k_{\text{THNF}}}{K_{\text{water}}}}{\left(1-\chi_{Ag}\right)\left[\left(1-\chi_{\text{Tio}_2}\right)\left[\left(1-\chi_{GO}\right)+\chi_{Ag}\frac{\left(\rho c_p\right)_{\text{Ag}}}{\left(\rho c_p\right)_{\text{water}}}\right]+\chi_{\text{Tio}_2}\frac{\left(\rho c_p\right)_{\text{Tio}_2}}{\left(\rho c_p\right)_{\text{water}}}\right]+\chi_{GO}\frac{\left(\rho c_p\right)_{\text{Tio}_2}}{\left(\rho c_p\right)_{\text{water}}}}\right)\frac{\partial^2 T}{\partial y^2}, \tag{7}$$

utilizing the boundary conditions as [33]:

$$U=U_w=aX,\ V=0,\ T=\frac{T-T_w}{T-T_\infty},\ \text{at } y=0$$
$$U\to U_e,\ T\to T_\infty \text{ as } Y\to\infty, \tag{8}$$

where χ_{Ag}, χ_{TiO_2}, and χ_{GO} are shown as the (NPs) volume fraction.

To gain (PDEs) from the previous dimensional equations, we illustrate the subsequent similarity transformations:

$$V=-\frac{\partial\psi}{\partial X},u=\frac{\partial\psi}{\partial Y}$$
$$\psi=(aV)^{\frac{1}{2}}Xf\left(\eta\right),\eta=(a/V)^{\frac{1}{2}}Y,\theta\left(\eta\right)=\frac{T-T_\infty}{T_\infty-T_w}. \tag{9}$$

ψ is the stream function. Hence, PDEs can be gotten as:

$$\frac{\rho_{\text{water}}}{\rho_{THNF}}\left[\frac{1}{\left(1-\chi_{Ag}\right)^{2.5}\left(1-\chi_{TiO_2}\right)^{2.5}\left(1-\chi_{GO}\right)^{2.5}}\right]\left(1+\frac{1}{\beta}\right)f'''+ff''-\left(f'\right)^2+$$
$$\left(\frac{1}{\rho_{THNF}}\left(1-\chi_{Ag}\right)\left[\left(1-\chi_{TiO_2}\right)\left[\left(1-\chi_{GO}\right)\rho_{\text{water}}+\chi_{GO}\frac{\rho_{GO}\beta_{GO}}{\beta_{\text{water}}}\right]+\chi_{TiO_2}\frac{\rho_{TiO_2}\beta_{TiO_2}}{\beta_{\text{water}}}\right]+\right. \tag{10}$$
$$\left.\chi_{Ag}\frac{\rho_{\text{Ag}}\beta_{Ag}}{\beta_{\text{water}}}\right)\lambda\theta+\left(\frac{a}{c}\right)^2+\frac{\rho_{\text{water}}}{\rho_{\text{THNF}}}\frac{\sigma_{\text{THNF}}}{\sigma_{\text{water}}}M\left(\frac{a}{c}-f'\right)=0,$$

$$\frac{1}{Pr_{\text{water}}}\left(\frac{\frac{k_{\text{THN}}}{k_{\text{water}}}}{\left(1-\chi_{\text{Ag}}\right)\left[\left(1-\chi_{\text{TiO}_2}\right)\left[\left(1-\chi_{GO}\right)+\chi_{GO}\frac{\left(\rho c_p\right)_{GO}}{\left(\rho c_p\right)_{\text{Water}}}\right]+\chi_{\text{TiO}_2}\frac{\left(\rho c_p\right)_{\text{TiO}_2}}{\left(\rho c_p\right)_{\text{water}}}\right]+\chi_{\text{Ag}}\frac{\left(\rho c_p\right)_{\text{Ag}}}{\left(\rho c_p\right)_{\text{water}}}}\right)(\theta'')$$
$$-f'\theta+f\theta'=0,$$

(11)

where

$$f(0)=0, f'(0)=1, \theta'(0)=1, \text{ at } \eta=0$$
$$f'(\eta)\to\frac{a}{c}, \theta(\eta)\to 0 \text{ at } \eta\to\infty^{*} \tag{12}$$

are the used boundary conditions.

$Pr_{\text{water}}=\frac{V_{\text{water}}}{k_{\text{water}}}$, $M=\frac{\sigma_{\text{water}}B_0^2a^2}{\rho_{\text{water}}V_{THNF}}$, are the Prandtl number, and magnetic parameter, respectively. a/c and λ are called stretching sheet and mixed convection parameters.

In this research, we are interested in well-known engineering quantities, such as Nu and the C_f, which explore the heat transfer that ensues via fluid convections. So, they can be presented as in:

$$C_f=\frac{\tau_w}{\rho U_w^2}, Nu=\frac{Xq_w}{k\left(\tau_w-\tau_{\text{infty}}\right)}. \tag{13}$$

Here, τ_w and q_w are determined to be shear stress and heat flux and are given as:

$$q_w=k_{THNF}\frac{\partial T}{\partial Y}, \tau_w=\mu_{THNF}\left(\frac{\partial U}{\partial Y}\right) \text{ at } Y=0. \tag{14}$$

So, C_f and Nu are expressed as:

$$C_f=\text{Re}e^{\frac{1}{2}}\left[\frac{1}{\left(1-\chi_{Ag}\right)^{2.5}\left(1-\text{TiO}_2\right)^{2.5}\left(1-\chi_{\text{TiO}_2}\right)^{2.5}}\right]\left(1+\frac{l}{\beta}\right)f''(0), Nu=\text{Re}^{\frac{1}{2}}\frac{k_{\text{THNF}}}{k_{\text{water}}}\theta'(0). \tag{15}$$

Reynolds number Re is known as $\frac{ax^2}{V_{\text{water}}}$.

3 Numerical Method and Accuracy

The Keller box method (KBM) is a numerical technique to study and find the solution of partial differential equations (PDEs) in heat transfer issues. Numerous advantages of KBM compared to different numerical procedures cause them more helpful and encourage investigators to employ them to solve heat transfer issues [34,35]. In this study, KBM procedures were utilized, as; reducing the PDEs degree. Linearize the consequent equations using Newton's method. Rearrange them in matrix-vector form, and solve this system using the block tridiagonal elimination technique. Once the dominant system of equations is solved numerically, and MATLAB code commands have been established, we ought to find accurate outcomes. So, it is needed to compare our results with previous results. So Table 1 shows the compared results between (Hassanien et al. [36], Salleh et al. [30]) studies and the special case of our investigation, which is Newtonian fluid when $\beta=\infty$, $\chi=\lambda=M=0$, $a/c=1$. Therefore, we got in good agreement outcomes. The (NPs) volume fraction is specified as $\chi=\chi_{Ag}=\chi_{TiO_2}=\chi_{GO}$. The thermal characteristics of the based fluid and the (NPs) operated in the existing investigation are presented in Table 2.

Table 1: Comparison of current outcomes with the previously issued investigation ($\beta = \infty, \chi = \lambda = M = 0, a/c = 1$), with several values of Pr

	Hassanien et al. [36]	Buongiorno [30]	Present
Pr	$-\theta'(0)$	$-\theta'(0)$	$-\theta'(0)$
0.72	0.46325	0.46317	0.46320
1	0.58198	0.58198	0.58197
3	1.16525	1.16522	1.16520
10	2.30801	2.30821	2.30814
100	7.74925	7.76249	7.73390

Table 2: Thermal characteristics of the based fluid and (NPs) [19,21]

Thermo-Physical feature	P (kg/m^3)	Cp (J/kg K)	K (W/m K)	βx10-5k-1	σ(s/m)	Pr
Ag	10500	235	429	1.89×10^{-5}	6.3×10^{7}	—
TiO_2	4250	686.2	0.9	0.9×10^{-5}	2.38×10^{6}	—
GO	1800	717	5000	28×10^{-5}	6.3×10^{7}	—
Water	997.1	4179	0.613	21×10^{-5}	5.5×10^{-6}	6.2

4 Results and Discussion

This section illustrates relevant parameters effects, such as the Casson parameter β, stretching sheet parameter a/c, mixed convection λ, (NPs) volume fraction parameter χ, and magnetic parameter M, upon the non-dimensional physical quantities, which are velocity $f'(\eta)$ and temperature $\theta(\eta)$, as well as local skin friction Cf and (Nu). It explores their examinations of flow features and heat transport by natural standards. $Ag - TiO_2$, and GO, suspended in water are employed as ternary (HNFs). The height in the β parameter declines the temperature profiles $\theta(\eta)$ and so for the lowering in the improvement in the thermal transfer of ternary (HNF). As the viscosity increases the liquid becomes more fluid and the temperature decreases and increases the velocity because of the effect cohesive forces between the molecules which overwhelm the transfer of molecular momentum between these molecules where the molecules being very close together (this explains why the volume of liquids is smaller than gases). In return, it registered that the temperature of (HNFs), $TiO_2 - GO$, was higher than that of ternary hybrid nanofluids, $Ag - TiO_2 - GO$, as presented in Fig. 2.

Similarly, in Fig. 3, the temperature profiles fall, when the stretching sheet parameter a/c increases. Besides that, the temperature profiles are not enhanced, when the addition of GO to (HNFs), $Ag - TiO_2$, to become ternary (HNFs) $Ag - TiO_2 - GO$.

The increase in the (NPs) volume fraction parameter χ, as shown in Fig. 4, led to a noticeable growth in temperature profiles. Here we see particles whose volume and temperature change, but whose pressure remains constant. So physical quantities, temperature, and velocity profiles of the ternary (HNFs) will be increased and decreased, respectively.

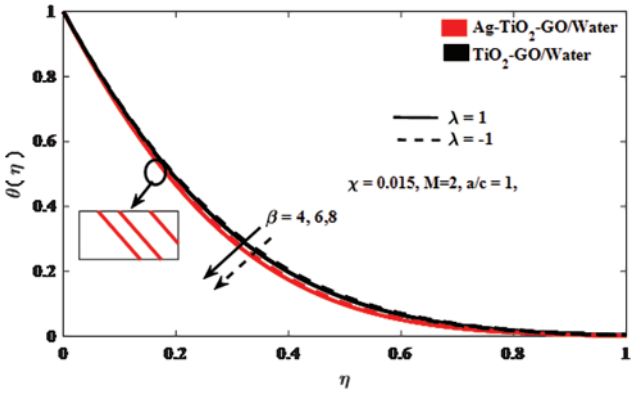

Figure 2: Temperature profiles *vs*. β

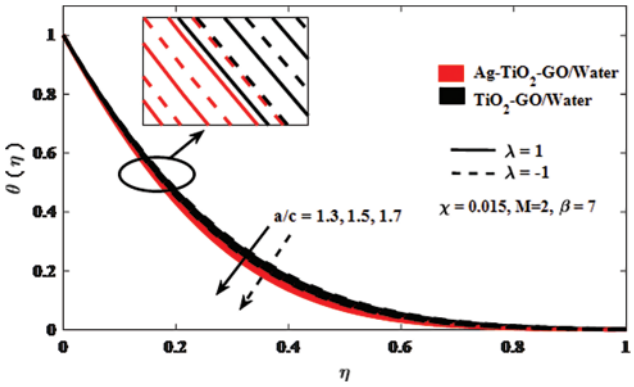

Figure 3: Temperature profiles *vs*. a/c

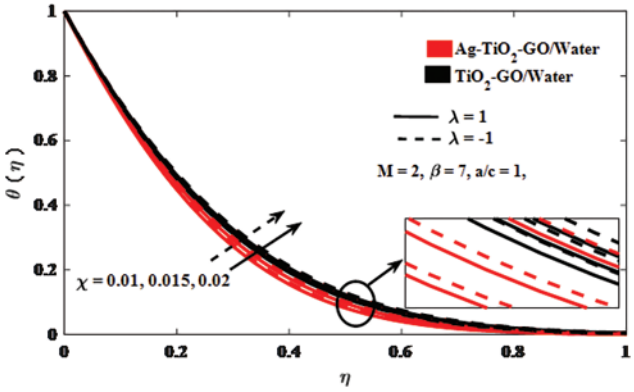

Figure 4: Temperature profiles *vs*. χ

Besides, when the ternary (HNFs) lost a particle GO, which gave us a higher temperature. Moreover, the magnetic parameter M increasing burns a rise in fluid motion, that is observed by a strengthened heat transfer, which implies increasing in temperature, as presented in Fig. 5. Due the higher the valence electrons into free electrons, the more temperatures are available to convert. Hence, the higher the temperature, the more free electrons are present in the lattice.

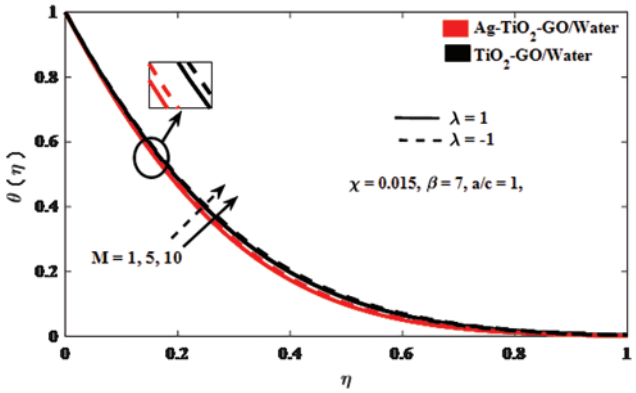

Figure 5: Temperature profiles *vs*. M

And it also viewed that the (HNF) temperature is higher than the ternary (HNFs temperature. While mixed convection parameter λ has a positive value equal to 1, this case is called heated convection flow. And the mixed convection parameter λ has a negative value equal to −1; this case is called cooled convection flow. Clarity, in all temperature profile Figs. 2–5, the negative value case has a higher temperature than the positive value case. And have the same behaviors in the decrements and increments in the two cases. The reliance of velocity profiles on the studied parameters is described in Figs. 6 to 9. In Fig. 6, when improving the Casson parameter β, in heated flow, it will be acquired that the velocity profiles will increase. Moreover, the increment in the viscosity points' strengths will grow and yield a low in the flow procedure. Specifically, it maintains the antagonism of the nanofluid's (NPs) to motion, which will reduce the velocity profiles. Also, the opposite demeanor completely happens, in the cooled flow case.

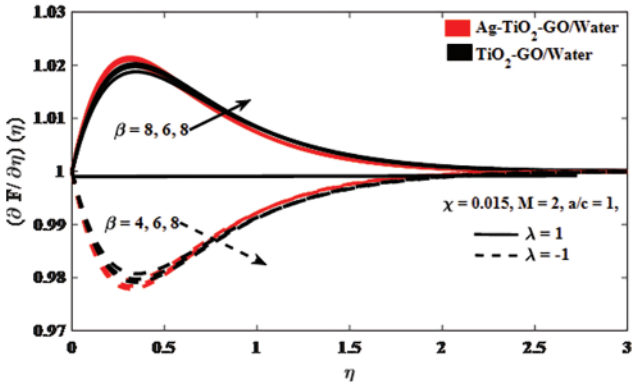

Figure 6: Velocity profiles *vs*. β

Fig. 7 illustrates the stretching sheet parameter a/c impact on the velocity profile, for $\lambda > 0$ and $\lambda < 0$. As seen in this figure by boosting the a/c, velocity profiles increase. Also, the ternary (HNFs) have a more heightened velocity than (HNFs).

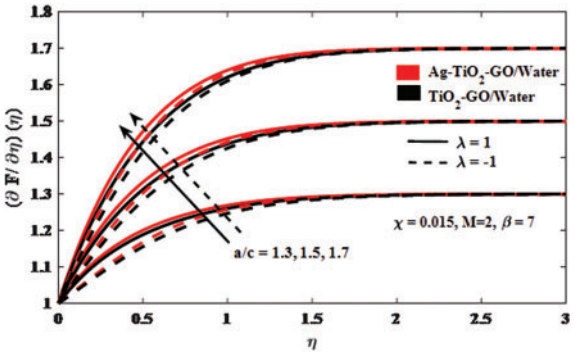

Figure 7: Velocity profiles *vs*. a/c

Figs. 8 and 9 present the conduct of (NPs) volume fraction and magnetic parameters M, respectively. It is recorded that, the increment of velocity profiles, in conjunction with the increase in these parameters, but in heated flow. Besides, it showed the high values of ternary (HNFs) *vs.* (HNFs). Moreover, the opposite marked case happens, in the cooled flow, the decrement of velocity profiles, in conjunction with the increase in these parameters. it is also clear that the high values of (HNFs) *vs.* ternary (HNFs)s.

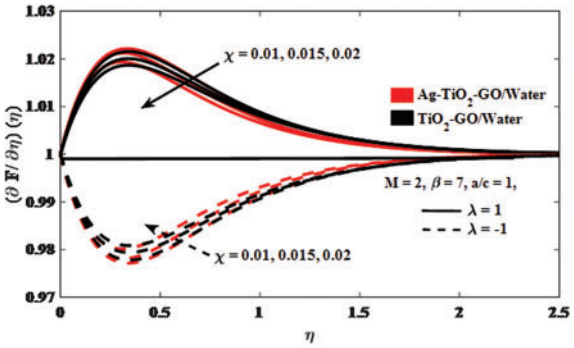

Figure 8: Velocity profiles *vs*. χ

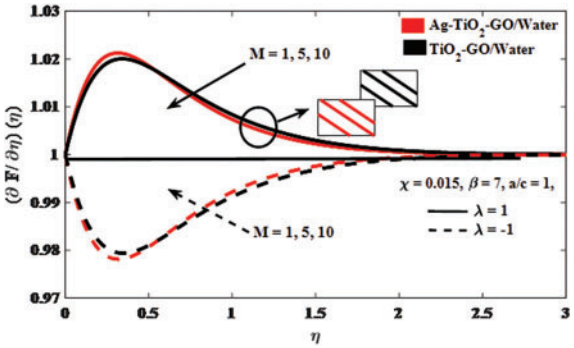

Figure 9: Velocity profiles *vs*. M

Table 3 displays local Cf and (Nu) values with different investigated parameters. It is obvious that Cf and Nu values are reduced when the values of the stretching sheet and Casson parameters are

raised, respectively. But the reverse happens, the Cf and Nu are incremented when these parameters are incremented. besides, all Cf and Nu values are improved when (NPs) volume fraction and magnetic parameters have risen. It is also noted that the Nu values of ternary (HNFs) are always higher than (HNFs). Cf for (HNFs) outcomes is higher than Cf for ternary (HNFs), with growing Casson and magnetic parameters values. Furthermore, the opposite case completely happens when we increase (NPs) volume fraction and stretching sheet parameters.

Table 3: Results of Nu and C_f with various significances β, a/c, χ, M, and λ = 1

				$Ag - TiO_2 - GO$ Water		$Ag - TiO_2$ Water	
β	a/c	χ	M	C_f	Nu	C_f	Nu
4				5.3648	2.3369	6.2590	1.7793
6	1	0.05	2	6.0125	2.001	7.5314	1.3247
8				7.2263	8.0178	8.0178	0.9950
	1.3	0.05			2.9863	6.0115	1.9368
7	1.5	2	6.6930	6.5897	3.2258	5.6987	2.4568
	1.8			6.1025	3.5897	5.1235	2.8763
		0.1		4.8987	2.7369	4.0087	2.3336
7	1	0.05	2	5.6697	3.5589	4.5519	2.7045
		0.08		6.7103	3.9703	5.1279	2.9703
			1	6.7789	1.9630	7.7789	2.9987
7	1	0.5	5	7.2758	2.6791	8.2581	3.6698
			10	7.6910	2.7893	8.3987	3.7963

5 Conclusion

The fundamental target of this work has been to demonstrate and discuss the behavior of mixed convection ternary (HNF) flow across a stretching sheet. The target has been achieved successfully, whereby the flow of $Ag - TiO_2$–GO water Casson Ternary (HNFs) in a Magneto-hydrodynamic Medium across a vertical stretching sheet is studied, where the boundary layer through a Casson medium and magnetohydrodynamics effects are considered. This system is solved by the Keller box method (KBM) numerically, where the outcome linear system of equations was programmed via MATLAB. The impacts of the relevant parameters, such as the Casson parameter β, stretching sheet parameter a/c, mixed convection λ, (NP) volume fraction parameter χ, and magnetic parameter M, upon the non-dimensional physical quantities, which are velocity $f'(\eta)$ and temperature $\theta(\eta)$, as well as local skin friction Cf and Nusselt number Nu. where the viscous dissipation effect is considered in magnetic field temperature profiles and velocity profiles which clarified in tables and figures and discussed in detail. Notably, the current work outcomes are in excellent agreement with earlier work outcomes.

Acknowledgement: Not applicable.

Funding Statement: This research was supported by Princess Nourah bint Abdulrahman University Researchers Supporting Project Number (PNURSP2025R522), Princess Nourah Bint Abdulrahman University, Riyadh, Saudi Arabia. This research is funded partially by Zarqa University-Jordan.

Author Contributions: The authors confirm contribution to the paper as follows: study conception and design: Munirah Alotaibi and Mohammed Z. Swalmeh; data collection: Munirah Alotaibi and Ahmed Hagag; analysis and interpretation of results: Mohammed Shqair and Mohammed Z. Swalmeh; draft manuscript preparation: Mohammed Shqair and Ahmed Hagag. All authors reviewed the results and approved the final version of the manuscript.

Availability of Data and Materials: Not applicable.

Ethics Approval: Not applicable.

Conflicts of Interest: The authors declare no conflicts of interest to report regarding the present study.

References

1. Yaw CT, Koh SP, Sandhya M, Kadirgama K, Tiong SK, Ramasamy D, et al. Heat transfer enhancement by hybrid nano additives? graphene nanoplatelets/cellulose nanocrystal for the automobile cooling system (radiator). Nanomaterials. 2023;13(5):808. doi:10.3390/nano13050808.
2. Poloju VK, Mukherjee S, Mishra PC, Aljuwayhel NF, Ali N. Efficient convective heat transfer enhancement in heat exchanger tubes with water based novel hybrid nanofluids: experimental investigation. J Therm Anal Calorim. 2023;148(15):7869–79. doi:10.1007/s10973-023-12251-9.
3. Alwawi FA, Al Faqih FM, Swalmeh MZ, Ibrahim MA. Combined convective energy transmission performance of Williamson hybrid nanofluid over a cylindrical shape with magnetic and radiation impressions. Mathematics. 2022;10(17):3191. doi:10.3390/math10173191.
4. Almse'adeen WA, Al Faqih FM, Swalmeh MZ. Magnetohydrodynamics boundary layer analysis of free convection flow in the presence of casson ternary hybrid nanofluid over a stretching sheet. In: The International Arab Conference on Mathematics and Computations; 2023; Singapore: Springer Nature Singapore. p. 563–77.
5. Madiwal S, Naduvinamani NB. Heat and mass transformation of casson hybrid nanofluid (MoS_2 + ZnO) based on engine oil over a stretched wall with chemical reaction and thermo-diffusion effect. Lubricants. 2024;12(6):221. doi:10.3390/lubricants12060221.
6. Akbar NS, Hussain MF, Alghamdi M, Muhammad T. Thermal characteristics of magnetized hybrid Casson nanofluid flow in a converging–diverging channel with radiative heat transfer: a computational analysis. Sci Rep. 2023;13(1):21891. doi:10.1038/s41598-023-49397-3.
7. Casson N. A Flow equation for pigment-oil suspensions of the printing ink-type. Rheology of disperse systems. In: Mill CC, editor. Rheology of disperse systems. Oxford: Pergamon Press; 1959. p. 84–104.
8. EL-Kabeir SM, El-Zahar ER, Rashad AM. Effect of chemical reaction on heat and mass transfer by mixed convection flow of casson fluid about a sphere with partial slip. J Comput Theor Nanosci. 2016;13(8):5218–26. doi:10.1166/jctn.2016.5405.
9. Khan MW, Ali N. Theoretical analysis of thermal entrance problem for blood flow: an extension of classical Graetz problem for Casson fluid model using generalized orthogonality relations. Int Commun Heat Mass Transf. 2019;109(13):104314. doi:10.1016/j.icheatmasstransfer.2019.104314.

10. Hamarsheh AS, Alwawi FA, Alkasasbeh HT, Rashad AM, Idris R. Heat transfer improvement in MHD natural convection flow of graphite oxide/carbon nanotubes-methanol based Casson nanofluids past a horizontal circular cylinder. Processes. 2020;8(11):1444. doi:10.3390/pr8111444.
11. Yusof NS, Soid SK, Illias MR, Abd Aziz AS, Nasir NA. Radiative boundary layer flow of Casson fluid over an exponentially permeable slippery Riga plate with viscous dissipation. J Adv Res Appl Sci Eng Technol. 2020;21(1):41–51. doi:10.37934/araset.21.1.4151.
12. Al-Hanaya A, Alotaibi M, Shqair M, Hagag AE. MHD effects on Casson fluid flow squeezing between parallel plates. AIMS Math. 2023;8(12):29440–52. doi:10.3934/math.20231507.
13. Pop I, Sheremet M. Free convection in cavity filled with a Casson fluid under the effects of thermal radiation and viscous dissipation. Int J Num Meth Heat Flu Flow. 2017;27(10):2318–32. doi:10.1108/HFF-09-2016-0352.
14. Khan SI, Khan U, Ahmed N, Jan SU, Waheed A, Mohyud-Din ST. Effects of viscous dissipation and convective boundary conditions on Blasius and Sakiadis problems for Casson fluid. Natl Acad Sci Lett. 2015;38(3):247–50. doi:10.1007/s40009-014-0331-7.
15. Hayat T, Khan MI, Waqas M, Yasmeen T, Alsaedi A. Viscous dissipation effect in flow of magneto-nanofluid with variable properties. J Mol Liq. 2016;222:47–54. doi:10.1016/j.molliq.2016.06.096.
16. Barik RN, Dash GC. Thermal radiation effect on an unsteady magnetohydrodynamic flow past inclined porous heated plate in the presence of chemical reaction and viscous dissipation. Appl Math Comput. 2014;226(12):423–34. doi:10.1016/j.amc.2013.09.077.
17. Qasim M, Noreen S. Heat transfer in the boundary layer flow of a Casson fluid over a permeable shrinking sheet with viscous dissipation. Eur Phys J Plus. 2014;129(1):1–8. doi:10.1140/epjp/i2014-14007-5.
18. Medikare M, Joga S, Chidem KK. MHD stagnation point flow of a Casson fluid over a nonlinearly stretching sheet with viscous dissipation. Am J Comput Math. 2016;6(1):37. doi:10.4236/ajcm.2016.61005.
19. Minakov AV, Rudyak VY, Pryazhnikov MI. Systematic experimental study of the viscosity of nanofluids. Heat Transf Eng. 2021;42(12):1024–40. doi:10.1080/01457632.2020.1766250.
20. Jamshed W, AkgÃŒl EK, Nisar KS. Keller box study for inclined magnetically driven Casson nanofluid over a stretching sheet: single phase model. Phys Scr. 2021;96(6):065201. doi:10.1088/1402-4896/abecfa.
21. Alwawi FA, Swalmeh MZ. Numerical study on the characteristics of heat transport through a trihybrid Jeffrey nanoliquid flowing about a radiant and magnetized cylinder. Proc Instit Mech Eng Part E: J Process Mech Eng. 2024. doi:10.1177/09544089241279.
22. Farooq U, Waqas H, Aldhabani MS, Fatima N, Alhushaybari A, Ali MR, et al. Modeling and computational framework of radiative hybrid nanofluid configured by a stretching surface subject to entropy generation: using Keller box scheme. Arab J Chem. 2023;16(4):104628. doi:10.1016/j.arabjc.2023.104628.
23. Alzu'bi OA, Qabaah AS, Al Faqih FM, Yaseen N, Shawaqfeh SA, Swalmeh MZ. Newtonian heating on Casson mixed convection transport by ternary hybrid nanofluids over vertical stretching sheet: numerical study. J Adv Res Fluid Mech Thermal Sci. 2024;115(1):166–80. doi:10.37934/arfmts.115.1.166180.
24. Salleh MZ, Nazar R, Pop I. Mixed convection boundary layer flow about a solid sphere with Newtonian heating. Arch Mech. 2010;62(4):283–303.
25. Hayat T, Abbas Z, Pop I, Asghar S. Effects of radiation and magnetic field on the mixed convection stagnation-point flow over a vertical stretching sheet in a porous medium. Int J Heat Mass Transf. 2010;53(1–3):466–74. doi:10.1016/j.ijheatmasstransfer.2009.09.010.
26. Swalmeh MZ, Alwawi FA, Altawallbeh AA, Naganthran K, Hashim I. On the optimized energy transport rate of magnetized micropolar fluid via ternary hybrid ferro-nanosolids: a numerical report. Heliyon. 2023;9(12):e22553. doi:10.1016/j.heliyon.2023.e22553.
27. Khan KA, Jamil F, Ali J, Khan I, Ahmed N, Andualem M, et al. Analytical simulation of heat and mass transmission in Casson fluid flow across a stretching surface. Math Probl Eng. 2022. doi:10.1155/2022/5576194.

28. Merkin JH. Natural-convection boundary-layer flow on a vertical surface with Newtonian heating. Int J Heat Fluid Flow. 1994;15(5):392–8. doi:10.1016/0142-727X(94)90053-1.
29. Sandhya A, Ramana Reddy GV, Deekshitulu VSRG. Heat and mass transfer effects on MHD flow past an inclined porous plate in the presence of chemical reaction. Int J Appl Mech Eng. 2020;25(3):86–102. doi:10.2478/ijame-2020-0036.
30. Buongiorno J. Convective transport in nanofluids. J Heat Transfer. 2006;128(3):240–50. doi:10.1115/1.2150834.
31. Tiwari RK, Das MK. Heat transfer augmentation in a two-sided lid-driven differentially heated square cavity utilizing nanofluids. Int J Heat Mass Transf. 2007;50(9–10):2002–18. doi:10.1016/j.ijheatmasstransfer.2006.09.034.
32. Ali G, Kumam P, Sitthithakerngkiet K, Jarad F. Heat transfer analysis of unsteady MHD slip flow of ternary hybrid Casson fluid through nonlinear stretching disk embedded in a porous medium. Ain Shams Eng J. 2024;15(2):102419. doi:10.1016/j.asej.2023.102419.
33. Nazar R, Amin N, Pop I. Mixed convection boundary layer flow from a horizontal circular cylinder in micropolar fluSids: case of constant wall temperature. Int J Num Meth Heat Flu Flow. 2003;13(1):86–109. doi:10.1108/09615530310456778.
34. Sarif NM, Salleh MZ, Nazar R. Numerical solution of flow and heat transfer over a stretching sheet with Newtonian heating using the Keller box method. Procedia Eng. 2013;53(4):542–54. doi:10.1016/j.proeng.2013.02.070.
35. Jamshed W, Nisar KS. Computational single? phase comparative study of a Williamson nanofluid in a parabolic trough solar collector via the Keller box method. Int J Energy Res. 2021;45(7):10696–718. doi:10.1002/er.6554.
36. Hassanien IA, Abdullah AA, Gorla RS. Flow and heat transfer in a power-law fluid over a nonisothermal stretching sheet. Math Comput Model. 1998;28(9):105–16. doi:10.1016/S0895-7177(98)00148-4.